PTEP

Prog. Theor. Exp. Phys. **2013**, 073D01 (26 pages)
DOI: 10.1093/ptep/ptt045

Hadron–quark crossover and massive hybrid stars

Kota Masuda[1,2,*], Tetsuo Hatsuda[2,3], and Tatsuyuki Takatsuka[4†]

[1]*Department of Physics, The University of Tokyo, Tokyo 113-0033, Japan*
[2]*Theoretical Research Division, Nishina Center, RIKEN, Wako 351-0198, Japan*
[3]*Kavli IPMU, The University of Tokyo, Kashiwa 277-8583, Japan*
[4]*Iwate University, Morioka 020-8550, Japan*
*E-mail: masuda@nt.phys.s.u-tokyo.ac.jp

Received December 31, 2012; Accepted April 23, 2013; Published July 1, 2013

On the basis of the percolation picture from the hadronic phase with hyperons to the quark phase with strangeness, we construct a new equation of state (EOS) with the pressure interpolated as a function of the baryon density. The maximum mass of neutron stars can exceed $2M_\odot$ if the following two conditions are satisfied: (i) the crossover from hadronic matter to quark matter takes place at around three times the normal nuclear matter density, and (ii) the quark matter is strongly interacting in the crossover region and has a stiff equation of state. This is in contrast to the conventional approach, assuming the first-order phase transition in which the EOS always becomes soft due to the presence of the quark matter at high density. Although the choice of the hadronic EOS does not affect the above conclusion for the maximum mass, the three-body force among nucleons and hyperons plays an essential role in the onset of hyperon mixing and the cooling of neutron stars.

Subject Index D30, D33, D41, E32

1. Introduction

A neutron star (NS) is a cosmic laboratory that provides us with a testing ground for the rich phase structure of quantum chromodynamics (QCD) [1] through observables such as the mass (M), the radius (R), the surface temperature (T_s), the surface magnetic field (B_s), and so on [2]. Among others, M and R are particularly important probes for constraining the equation of state (EOS) and the composition of high-density matter.

From the theoretical point of view, the onset of the strangeness degrees of freedom inside NSs has attracted much attention in recent years: The general consensus is that hyperons (Y) such as Λ and Σ^- would participate in NS cores at densities of several times nuclear matter density ($\rho_0 = 0.17$ fm^{-3}) [3–9]. The precise value of the threshold density $\rho_{\rm th}$ depends on hyperon–nucleon interactions, which still show uncertainties at the moment but will be improved by future hypernuclear data [10–12] and by lattice QCD simulations [13]. From the observational point of view, a massive NS, PSR J1614-2230, with $M_{\rm obs} = (1.97 \pm 0.04)M_\odot$ was recently discovered [14]. Conflict between the $2M_\odot$ NS, which requires a stiff EOS, and Y-mixing, which gives a soft EOS, leads to the challenging problem of whether massive neutron stars are in contradiction with the existence of exotic components such as hyperons and deconfined quarks [15–23].

The purpose of the present paper is to investigate whether "hybrid stars", which have quark matter in the core, are compatible with a $2M_\odot$ NS. Historically, the transition from hadronic matter to quark

†These authors contributed equally to this work.

matter has been assumed to be a first-order phase transition and Gibbs phase equilibrium conditions are imposed. However, treating the point-like hadron as an independent degree of freedom is not fully justified in the transition region because all hadrons are extended objects composed of quarks and gluons. Furthermore, the system must be strongly interacting in the transition region, so that it can be described neither by an extrapolation of the hadronic EOS from the low-density side nor by an extrapolation of the quark EOS from the high-density side [24]. This is analogous to the BEC–BCS crossover realized in the many-body system of ultra-cold fermionic atoms [25].

Figure 1 illustrates the above situation in terms of the pressure as a function of baryon density (ρ). One may expect a gradual onset of quark degrees of freedom in dense matter associated with the percolation of finite-size hadrons, i.e., a smooth crossover from hadronic matter to quark matter. Such a percolation picture of hadrons has been discussed in seminal works such as Refs. [26,27]. Also, the hadron–quark continuity [28,29] and hadron–quark crossover [30,31] have been discussed in relation to the existence of color superconductivity at high density. In this paper, we show that the crossover picture can lead to a stiffening of the EOS, unlike the case of the first-order transition, if the following conditions are met: (i) the crossover takes place at relatively low density (around three times the normal nuclear matter density), and (ii) the strongly interacting quark matter has a stiff EOS. This implies that the hadron–quark crossover provides us with a novel mechanism to support massive neutron stars with quark cores. A preliminary account of our results has been reported in Ref. [33]. We note that an interpolation between hadronic matter and stiff quark matter was previously considered phenomenologically in Ref. [32].

This paper is organized as follows. In Sect. 2, the characteristic features of the hadronic EOSs (H-EOSs) to be used at low densities are summarized. In Sect. 3, we treat the strongly interacting quark matter by using a Nambu–Jona-Lasinio (NJL)-type model and derive the quark EOS (Q-EOS) to be used at high densities. In Sect. 4, we describe our interpolation procedure to obtain the EOS in the hadron–quark crossover region. In Sect. 5 and 6, numerical results and discussions are given for the bulk properties of hybrid stars, such as the M–R relationship, the maximum mass $M_{\rm max}$, and the M–ρ_c (central density) relationship. We discuss how these results depend on the different choice of H-EOS and Q-EOS. A comment on the cooling of NSs with respect to the hyperon mixture inside the core is also given. Section 7 is devoted to concluding remarks.

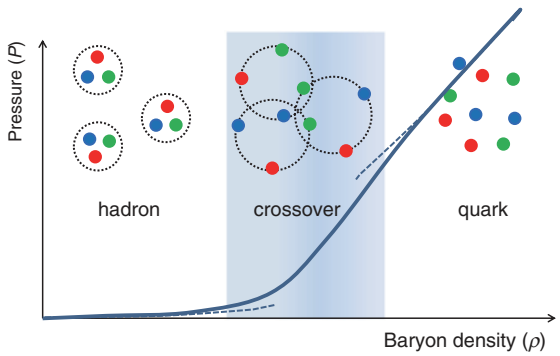

Fig. 1. Schematic picture of the QCD pressure (P) as a function of the baron density (ρ) under the assumption of the hadron–quark crossover. The crossover region where finite-size hadrons start to overlap and percolate is shown by the shaded area. The pressure calculated on the basis of point-like hadrons (shown by the dashed line at low density) and that calculated on the basis of weakly interacting quarks (shown by the dashed line at high density) lose their validity in the crossover region, so that the naive use of the Gibbs conditions by extrapolating the dashed lines is not justified in general.

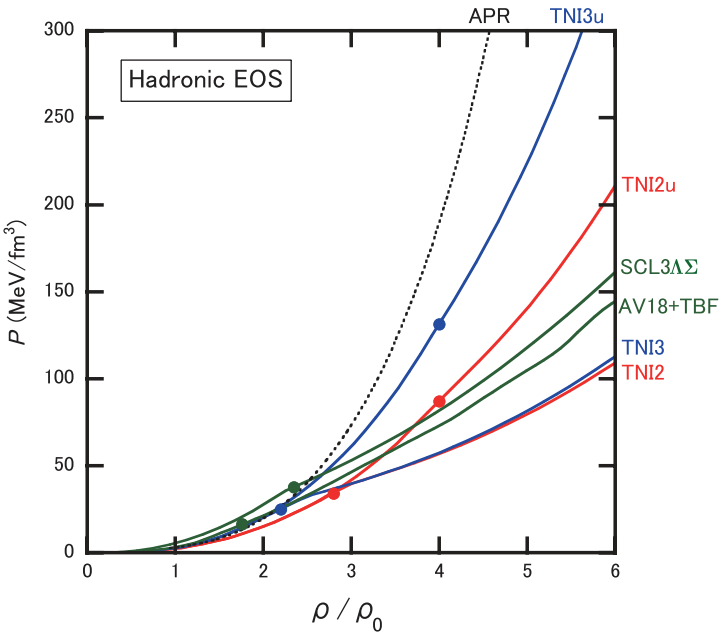

Fig. 2. Pressure (P) for Y-mixed neutron star matter with β-equilibrium and charge neutrality as a function of the total baryon density ρ for different types of EOS. Solid red lines: TNI2u (G-matrix approach, universal three-body force, $\kappa = 250$ MeV) and TNI2 (G-matrix approach, three-nucleon force, $\kappa = 250$ MeV). Solid blue lines: TNI3u (G-matrix approach, universal three-body force, $\kappa = 300$ MeV) and TNI3 (G-matrix approach, three-nucleon force, $\kappa = 300$ MeV) [34,35]. Solid green lines: AV18+TBF (G-matrix approach, three-nucleon force, $\kappa = 192$ MeV) [37] and SCL3$\Lambda\Sigma$ (relativistic mean field model with chiral SU(3) symmetry, $\kappa = 211$ MeV) [40]. Paris+TBF is not plotted here because it is almost the same as AV18+TBF. For comparison, P for the neutron star matter without hyperons obtained from APR EOS [41] is also shown by the dotted lines.

2. Hadronic EOS (H-EOS)

We consider several different EOSs with Y-mixing:

- TNI2, TNI3, TNI2u, and TNI3u [34,35]: TNI2 and TNI3 are obtained by the G-matrix calculation with a Reid soft-core potential for NN and a Nijmegen type-D hard-core potential for YN and YY. Also, a phenomenological three-body force [36] is introduced in the form of an effective NN force to reproduce the saturation point of symmetric nuclear matter with the incompressibility $\kappa = 250$ MeV (TNI2) and $\kappa = 300$ MeV (TNI3). For TNI2u and TNI3u, the three-body interaction is introduced *universally* in the form of effective NN, NY, and YY forces.
- AV18+TBF and Paris+TBF [37]: These are obtained by the G-matrix calculation but with a different choice of potentials; AV18 and Paris potentials for NN and a Nijmegen soft-core potential for YN and YY. Also, a three-body force of Urbana type is introduced in the form of an effective NN force to meet the saturation condition.
- SCL3$\Lambda\Sigma$ [40]: This is based on a relativistic mean field (RMF) model with chiral SU(3) symmetry and logarithmic potential motivated by the strong coupling lattice QCD approach. The phenomenological parameters of the model are determined to reproduce the saturation condition, bulk properties of normal nuclei, and separation energies of single- and double-Λ hypernuclei.

In Fig. 2, we plot the pressure P for Y-mixed neutron star matter with β-equilibrium and charge neutrality as a function of baryon density ρ obtained from the EOSs listed above (Paris+TBF is not shown since it is almost the same as AV18+TBF). For comparison, P for neutron star matter without

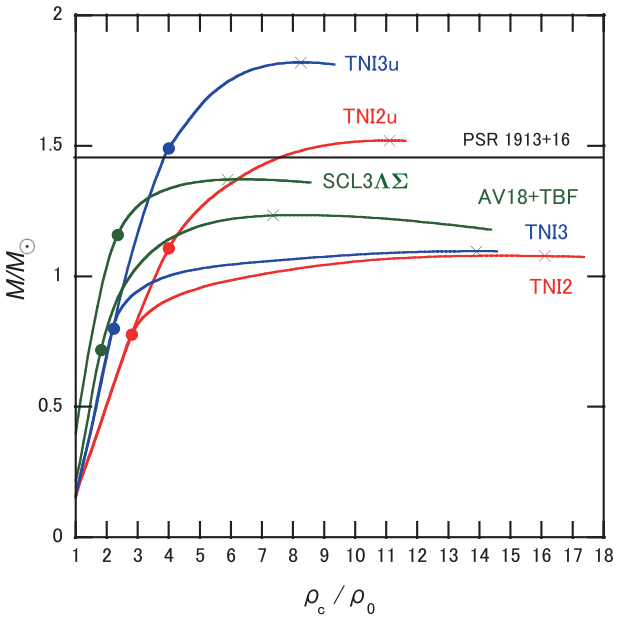

Fig. 3. M–ρ_c relationship corresponding to the EOSs in Fig. 2 (details of the EOSs are given in Table A1 of Appendix A). The colors on each line are the same as those in Fig. 2. The cross symbols denote the points where the NS mass becomes maximum, $M_{\rm max}$. The solid black line denotes $M = 1.44 M_\odot$ for PSR 1913+16.

Table 1. Properties of various hadronic EOSs with hyperons: TNI2, TNI3, TNI2u, TNI3u [34,35], Paris+TBF, AV18+TBF [37–39], and SCL3ΛΣ [40]. κ is the nuclear incompressibility and $\rho_{\rm th}$ is the threshold density of hyperon-mixing with ρ_0 ($= 0.17/\text{fm}^3$) being the normal nuclear density. R and ρ_c denote the radius and central density for the maximum mass ($M_{\rm max}$) NS, respectively. The numbers in parentheses are those without hyperons. *indicates that the numbers are taken from the figures in Ref. [37].

EOS	TNI2	TNI3	TNI2u	TNI3u	Paris+TBF	AV18+TBF	SCL3ΛΣ
κ (MeV)	250	300	250	300	281	192	211
$\rho_{\rm th}(\Lambda)/\rho_0$	2.95	2.45	4.01	4.01	2.9*	2.8*	2.24
$\rho_{\rm th}(\Sigma^-)/\rho_0$	2.83	2.23	4.06	4.01	1.9*	1.8*	2.24
$M_{\rm max}/M_\odot$	1.08	1.10	1.52	1.83	1.26	1.22	1.36
	(1.62)	(1.88)			(2.06)	(2.00)	(1.65)
R (km)	7.70	8.28	8.43	9.55	10.46	10.46	11.42
	(8.64)	(9.46)			(10.50)	(10.54)	(10.79)
ρ_c/ρ_0	16.10	13.90	11.06	8.26	7.35	7.35	6.09
	(9.97)	(8.29)			(6.47)	(6.53)	(6.85)

hyperons obtained from the APR EOS ([41]) is also plotted in Fig. 2 with dotted lines. In Fig. 3, the M–ρ_c relationships for the corresponding NS models are shown. The filled circle on each curve denotes the threshold density of the Y-mixture. There are some features to be noted in the figure: (i) Different H-EOSs do not show a significant difference in P up to 2.5 ρ_0, and (ii) the Y-mixture is delayed from (2–3)ρ_0 to 4ρ_0 if a repulsive three-body force exists universally for baryons, as in the case of TNI2u and TNI3u. Even light-mass NSs ($M < M_\odot$ for TNI2, TNI3, and AV18+TBF and $M < 1.2 M_\odot$ for SCL3ΛΣ) already have Y-mixed cores.

In Table 1, we show κ and the threshold densities of hyperon-mixing, $\rho_{\rm th}(\Lambda)$ and $\rho_{\rm th}(\Sigma^-)$, for each H-EOS. In the same table, we show the maximum-mass $M_{\rm max}$, the radius R, and the central density $\rho_{\rm c}$ of the NS obtained from each H-EOS. The values obtained by switching off the Y-mixing are given in parentheses for comparison. For the H-EOSs without universal three-body repulsion, significant

softening due to Y-mixing reduces $M_{\max}$, i.e., $M_{\max}$ (without Y) $= (1.62\text{–}2.00)M_\odot$, $(1.08\text{–}1.26) \to (1.08\text{–}1.26)M_\odot$. This clearly contradicts the observed mass $M_{\rm obs} = 1.44M_\odot$ for PSR1913+16. On the other hand, for H-EOSs with universal three-body repulsion (TNI2u, TNI3u), $M_{\max}$ has almost recovered to that without Y.

The use of the several kinds of EOS mentioned above, from different theoretical methods (G-matrix, RMF), with various stiffness values ranging from $\kappa \sim 190$ MeV to 300 MeV and with the variation of $\rho_{\rm th}(Y) \simeq (2-4)\rho_0$, is expected to cover the present uncertainties of the H-EOSs. For completeness, numerical values of the pressure P and the energy density ε as a function of the baryon density are tabulated in Table A1 in Appendix A.

3. Quark EOS (Q-EOS)

The baryon density at the central core of the NSs would be at most $10\rho_0$. Although hadrons do not keep their identities in such a high density, the chemical potentials of the quarks are about (400–500) MeV, which is not high enough for the asymptotic freedom at work. Namely, the deconfined quarks inside the NSs, even if they exist, would be strongly interacting. An analogous situation at finite temperature is expected theoretically and has recently been confirmed by the relativistic heavy-ion collisions at RHIC and LHC; it is now called the strongly interacting quark–gluon plasma (sQGP).

Since lattice QCD to treat the strongly interacting quark matter (sQM) at finite baryon density is unfortunately not possible due to the notorious sign problem, we adopt an effective theory of QCD, the $(2+1)$-flavor Nambu–Jona-Lasinio (NJL) model. This model is particularly useful for taking into account important phenomena such as the partial restoration of chiral symmetry at high density [42–45].

The model Lagrangian we consider is

$$\mathcal{L}_{\rm NJL} = \overline{q}(i\partial\!\!\!/ - m)q + \frac{1}{2}G_S\sum_{a=0}^{8}[(\overline{q}\lambda^a q)^2 + (\overline{q}i\gamma_5\lambda^a q)^2] - G_D[\det\overline{q}(1+\gamma_5)q + \text{h.c.}] - \begin{cases} \frac{1}{2}g_V(\overline{q}\gamma^\mu q)^2 \\ \frac{1}{2}G_V\sum_{a=0}^{8}\left[(\overline{q}\gamma^\mu\lambda^a q)^2 + (\overline{q}i\gamma^\mu\gamma_5\lambda^a q)^2\right] \end{cases} \tag{1}$$

where the quark field q_i $(i = u, d, s)$ has three colors and three flavors with the current quark mass m_i. The term proportional to G_S is a $U(3)_L \times U(3)_R$ symmetric four-fermi interaction where λ^a are the Gell-Mann matrices with $\lambda^0 = \sqrt{2/3}$ I. The term proportional to G_D is the Kobayashi–Maskawa–'t Hooft (KMT) six-fermi interaction, which breaks $U(1)_A$ symmetry. We consider two types of vector interaction (the second line of Eq. (1)): The term proportional to $g_V(>0)$ gives a universal repulsion among different flavors, while the one proportional to $G_V(>0)$ gives flavor-dependent repulsion.

In the mean-field approximation, the constituent quark masses M_i $(i = u, d, s)$ are generated dynamically through the NJL interactions $(G_{S,D})$:

$$M_i = m_i - 2G_S\sigma_i + 2G_D\sigma_j\sigma_k, \tag{2}$$

where $\sigma_i = \langle\bar{q}_i q_i\rangle$ is the quark condensate in each flavor, and (i, j, k) corresponds to the cyclic permutation of u, d, and s. The thermodynamic potential Ω is related to the pressure as $\Omega = -T$ log

Table 2. Parameter sets of the $(2+1)$-flavor NJL model [42–45].

	Λ (MeV)	$G_S\Lambda^2$	$G_D\Lambda^5$	$m_{u,d}$ (MeV)	m_s (MeV)
HK	631.4	3.67	9.29	5.5	135.7
RKH	602.3	3.67	12.36	5.5	140.7
LKW	750	3.64	8.9	3.6	87

$Z = -PV$, so that we have

$$P(T,\mu_{u,d,s}) = T\sum_i\sum_\ell\int\frac{d^3p}{(2\pi)^3}\mathrm{Trln}\left(\frac{S_i^{-1}(i\omega_\ell,\mathbf{p})}{T}\right) - G_S\sum_i\sigma_i^2 - 4G_D\sigma_u\sigma_d\sigma_s + \begin{cases}\frac{1}{2}g_V\left(\sum_i n_i\right)^2\\ \frac{1}{2}G_V\sum_i n_i^2\end{cases} \tag{3}$$

where $n_i = \langle q_i^\dagger q_i\rangle$ is the quark number density in each flavor, and S_i is the quark propagator, which can be written as

$$S_i^{-1} = \not{p} - M_i - \gamma^0\mu_i^{\mathrm{eff}}, \quad \mu_i^{\mathrm{eff}} \equiv \begin{cases}\mu_i - g_V\sum_j n_j\\ \mu_i - G_V n_i\end{cases} \tag{4}$$

where $i\omega_\ell = (2\ell+1)\pi T$ and μ_i^{eff} is an effective chemical potential [46].

There are six independent parameters in the (2+1)-flavor NJL model: the UV cutoff, Λ, the coupling constants, G_S, G_D, and $g_V(G_V)$, and the quark masses, $m_{u,d}$ and m_s. Five parameters except for $g_V(G_V)$ have been determined from hadron phenomenology. We consider three parameter sets, summarized in Table 2: HK (Hatsuda and Kunihiro), RKH (Rehberg, Klevansky, and Hufner) and LKW (Lutz, Klimt, and Weise) [42–45].

The magnitude of $g_V(G_V)$ has not been determined well: Recent studies of the Polyakov-Nambu-Jona-Lasinio model applied to the QCD phase diagram suggest that g_V may be comparable to or larger than G_S [47,48], so that we change its magnitude in the following range:

$$0 \le \frac{g_V}{G_S} \le 1.5. \tag{5}$$

In Sects 5 and 6, we will show our results mainly for the HK parameter set with the vector interaction of the g_V type. At the end of Sect. 5, we discuss how the results change in other cases. The Q-EOS with strangeness is obtained from the above model under two conditions: (i) charge neutrality among quarks and leptons, i.e. $\frac{2}{3}n_u - \frac{1}{3}n_d - \frac{1}{3}n_s - n_e - n_\mu = 0$, and (ii) the β-equilibrium among quarks and leptons, i.e. $\mu_d = \mu_s = \mu_u + \mu_e$ and $\mu_e = \mu_\mu$.

In Fig. 4, the number fractions ($n_{u,d,s,e}/n_{\mathrm{tot}}$ with $n_{\mathrm{tot}} = n_u + n_d + n_s = 3\rho$) as a function of the baryon density ρ are plotted. Also, in Fig. 5, the constituent quark masses (M_i) as a function of ρ are plotted. The HK parameter set with the g_V-type interaction is used in both figures. The flavor-independent g_V-type interaction leads to a pressure in Eq. (3) depending only on μ_i^{eff}. Then, the number fractions and the quark masses as a function of ρ do not depend on g_V.

At low baryon densities below a threshold density $\rho_{\mathrm{th}} \simeq 4\rho_0$, the system is composed of only u, d, and e with $n_d \sim 2n_u$ due to charge neutrality and β-equilibrium (Fig. 4). In this region, the strong interaction among quarks (mainly the G_S term in the NJL model) drives the partial restoration of

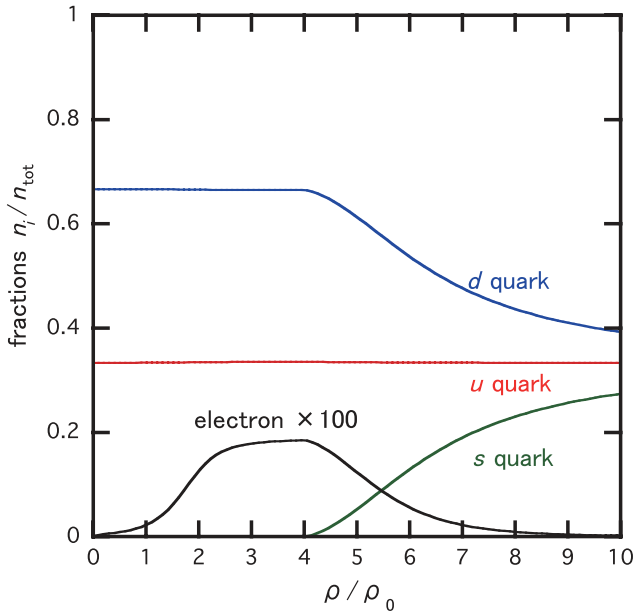

Fig. 4. The number fractions ($n_{u,d,s,e}/n_{\rm tot}$ with $n_{\rm tot} = n_u + n_d + n_s = 3\rho$) as a function of the baryon density ρ. Solid red line: The fraction of u quarks. Solid blue line: The fraction of d quarks. Solid green line: The fraction of s quarks. Solid black line: The fraction of the electron × 100. The muon does not appear due to the emergence of s quarks.

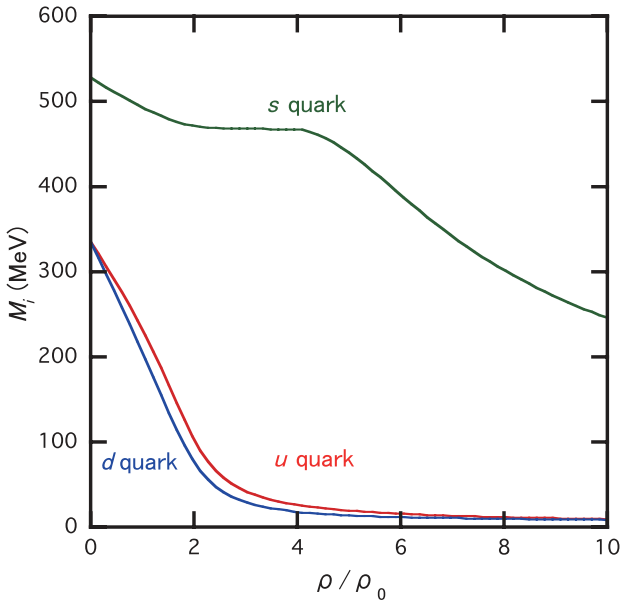

Fig. 5. The constituent quark masses (M_i) as a function of ρ. The colors of each line are the same as those in Fig. 4.

chiral symmetry and hence a rapid decrease of the constituent masses $M_{u,d}$ (Fig. 5). Due to the coupling between different flavors through the G_D term, the strange quark mass M_s in the Dirac sea is also affected slightly.

When the baryon density exceeds $\rho_{\rm th}$, the chemical potential of the strange quark μ_s becomes larger than the strange quark mass ($\mu_s > M_s$), so that the system starts to have the strangeness degree of freedom. Since the strange quark is negatively charged, electrons start to disappear from the system

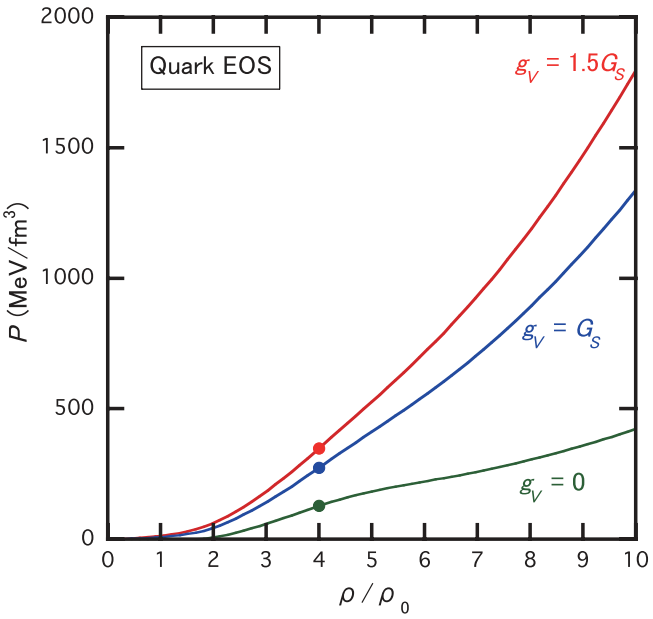

Fig. 6. Pressure (P) as a function of baryon density ρ in a pure quark matter for the HK parameter set with $g_V/G_S = 0, 1.0, 1.5$. The filled circles denote the onset of strangeness.

and the d quark fraction decreases at the same time (Fig. 4). We note that the system does not have the muon, because the electron chemical potential is smaller than $m_\mu = 106\,\text{MeV}$ at all densities. In the high-density limit, the system approaches the flavor-symmetric u, d, s matter without leptons. Once the s-quark appears in the system, M_s is also suppressed, mainly due to the G_S term (Fig. 5). The strangeness threshold ρ_{th} does not depend on g_V as already mentioned, but it does depend on the NJL parameter sets in Table 2: $\rho_{\text{th}}/\rho_0 = 4.0$, 3.9, and 3.0 for HK, RKH, and LKW, respectively.

In Fig. 6, we plot the pressure ($P(\rho)$ with a normalization $P(0) = 0$) of the strongly interacting quark matter for the HK parameter set with different values of the vector coupling ($g_V/G_S = 0, 1.0, 1.5$ according to Eq. (5)). Due to the universal repulsion of the g_V-type vector interaction, the Q-EOS becomes stiffer as g_V increases. As already mentioned, the onset density of the strangeness (shown by the filled circles) does not depend on g_V. We note here that the present Q-EOS has a first-order phase transition below $2\rho_0$ for $g_V < 0.3G_S$. However, it does not affect the final results of the present paper, since such a low-density region is dominated by the hadronic EOS in our hadron–quark crossover approach, to be discussed in Sect. 4.

4. Hadron–quark crossover

As discussed in Sect. 1, treating the point-like hadron as an independent degree of freedom loses its validity as the baryon density approaches the percolation region. In other words, the system can be described neither by an extrapolation of the hadronic EOS from the low-density side nor by an extrapolation of the quark EOS from the high-density side. Under such a situation, it does not make much sense to apply the Gibbs criterion of two phases I and II, $P_{\text{I}}(T_c, \mu_c) = P_{\text{II}}(T_c, \mu_c)$, since P_{I} and P_{II} are not reliable in the transition region.

Since a first-principles QCD calculation at high baryon density is not available and effective models at finite baryon density with proper treatment of the confinement phenomena do not exist at present, we will consider a phenomenological "interpolation" between the H-EOS and Q-EOS as a first

step. Such an interpolation is certainly not unique: Here we consider the two simplest possibilities, P-interpolation and ε-interpolation, as described below.

- P-interpolation as a function of baryon density:

$$P(\rho) = P_H(\rho) f_-(\rho) + P_Q(\rho) f_+(\rho), \tag{6}$$

$$f_\pm(\rho) = \frac{1}{2}\left(1 \pm \tanh\left(\frac{\rho - \bar{\rho}}{\Gamma}\right)\right), \tag{7}$$

where P_H and P_Q are the pressure in the hadronic matter and that in the quark matter, respectively. An interpolating function $f_\pm$ similar to ours has been previously considered at finite temperature in Refs. [49–51]. The window $\bar{\rho} - \Gamma \lesssim \rho \lesssim \bar{\rho} + \Gamma$ characterizes the crossover region in which both hadrons and quarks are strongly interacting, so that neither the pure hadronic EOS nor the pure quark EOS are reliable. The percolation picture illustrated in Fig. 1 is best implemented by the interpolation in terms of the baryon density ρ instead of the baryon chemical potential. One should not confuse Eq. (7) with the pressure in the mixed phase associated with the first-order phase transition in which $f_\pm$ is considered to the volume fraction of each phase. In our crossover picture, the system is always uniform and f_- (f_+) should be interpreted as the degree of reliability of H-EOS (Q-EOS) at a given baryon density.

To calculate the energy density ε as a function of ρ in a thermodynamically consistent way, we integrate the thermodynamical relation $P = \rho^2 \partial(\varepsilon/\rho)/\partial\rho$ and obtain

$$\varepsilon(\rho) = \varepsilon_H(\rho) f_-(\rho) + \varepsilon_Q(\rho) f_+(\rho) + \Delta\varepsilon \tag{8}$$

$$\Delta\varepsilon = \rho \int_{\bar{\rho}}^{\rho} (\varepsilon_H(\rho') - \varepsilon_Q(\rho')) \frac{g(\rho')}{\rho'} d\rho' \tag{9}$$

with $g(\rho) = \frac{2}{\Gamma}(e^X + e^{-X})^{-2}$ and $X = (\rho - \bar{\rho})/\Gamma$. Here ε_H (ε_Q) is the energy density obtained from H-EOS (Q-EOS). $\Delta\varepsilon$ is an extra term that guarantees thermodynamic consistency. Note that the energy per baryon from the extra term $\Delta\varepsilon/\rho$, which receives its main contribution from the crossover region, is finite even in the high-density limit.

- ε-interpolation as a function of baryon density:

$$\varepsilon(\rho) = \varepsilon_H(\rho) f_-(\rho) + \varepsilon_Q(\rho) f_+(\rho). \tag{10}$$

Other thermodynamic quantities are obtained through the thermodynamic relation

$$P(\rho) = P_H(\rho) f_-(\rho) + P_Q(\rho) f_+(\rho) + \Delta P \tag{11}$$

$$\Delta P = \rho(\varepsilon_Q(\rho) - \varepsilon_H(\rho)) g(\rho), \tag{12}$$

and $\mu = (\varepsilon + P)/\rho$. Here ΔP is an extra term that guarantees thermodynamic consistency; it is a localized function in the crossover region and obeys the property $\Delta P(0) = \Delta P(\infty) = 0$.

5. Neutron star properties with P-interpolation

5.1. *Interpolated EOS*

In the present section we consider the case of P-interpolation. The case of ε-interpolation will be discussed in Sect. 6. We note that the crossover window in both interpolations should satisfy the following physical conditions: (i) The system is always thermodynamically stable, $dP/d\rho > 0$, and (ii) the normal nuclear matter is well described by the H-EOS so that $\bar{\rho} - 2\Gamma > \rho_0$ is satisfied.

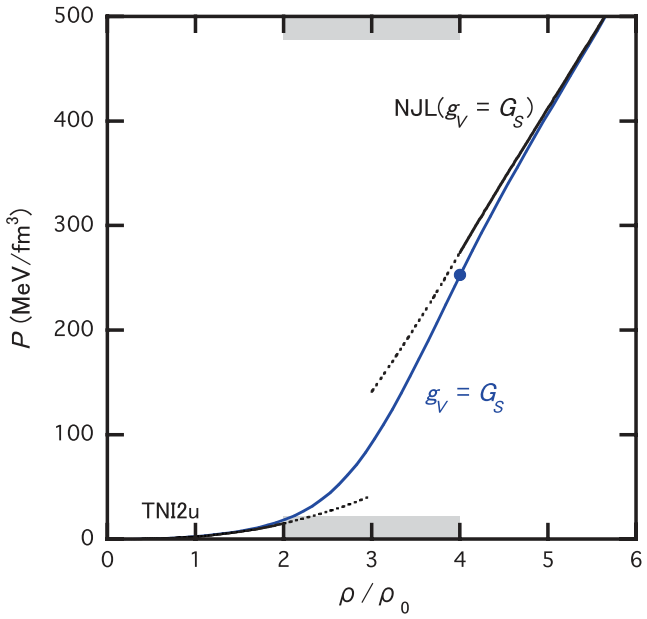

Fig. 7. The interpolated pressure between TNI2u H-EOS and NJL Q-EOS with $g_V = G_S$ for $(\bar{\rho}, \Gamma) = (3\rho_0, \rho_0)$. Pressure is illustrated by a blue line. The filled circle denotes the threshold density of strangeness.

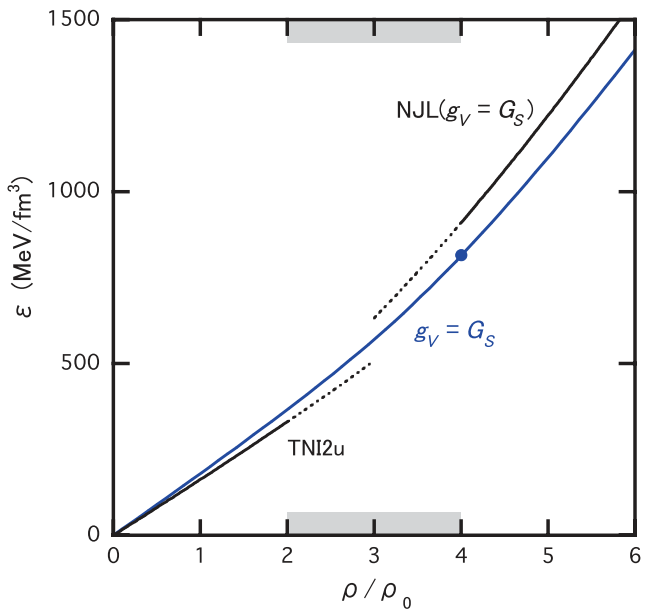

Fig. 8. The energy density obtained from the interpolated pressure in Fig. 7. Energy density is illustrated by a blue line. The filled circle denotes the threshold density of strangeness.

Shown in Figs. 7–9 are examples of the P-interpolation between TNI2u for H-EOS and NJL with $g_V = G_s$ for Q-EOS according to Eq. (7). The crossover window is chosen to be $(\bar{\rho}, \Gamma) = (3\rho_0, \rho_0)$ and is shown by the shaded area on the horizontal axis. An important lesson that one can learn from Fig. 7 is that the H-EOS (Q-EOS) is nothing more than the asymptotic form of the "true"

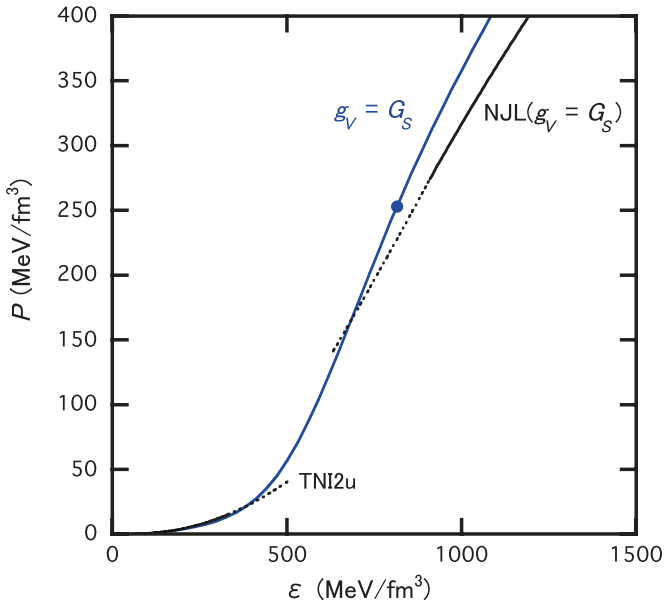

Fig. 9. The relation between interpolated pressure and energy density. The parameters are the same as in Fig. 7. The filled circle denotes the threshold density of strangeness.

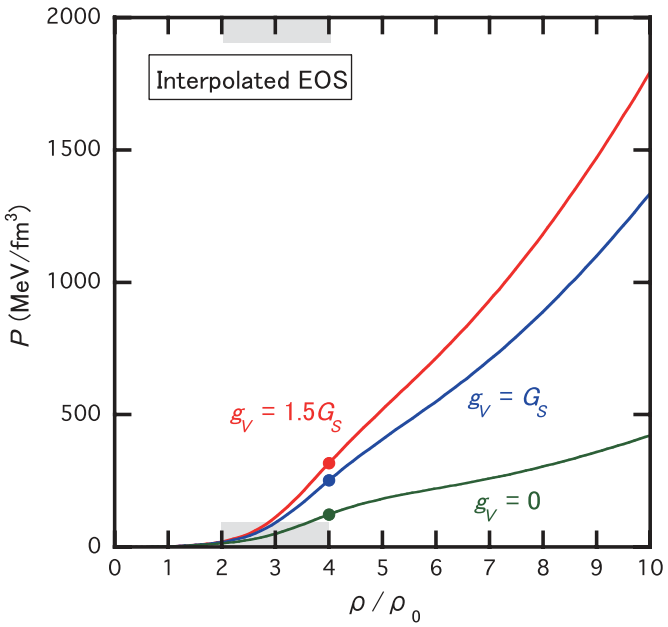

Fig. 10. Interpolated pressure (P) as a function of baryon density ρ for the case $(\bar{\rho}, \Gamma) = (3\rho_0, \rho_0)$ with $g_V/G_S = 0, 1.0, 1.5$.

$P(\rho)$ around $\rho = 0$ ($\rho = \infty$). Therefore, naive extrapolation of H-EOS and Q-EOS beyond their applicability would miss essential physics.

In Fig. 10, we plot the interpolated EOS using TNI2u and NJL for different values of g_V in a wide range of baryon density. The filled circles denote the onset of strangeness degrees of freedom, either hyperons or strange quarks.

Table 3. $M_{\max}/M_\odot$ (ρ_c/ρ_0) for different choices of H-EOS and different stiffness values for Q-EOS.

H-EOS	$g_V = G_S$	$g_V = 1.5G_S$
TNI2u	2.05 (6.1)	2.17 (5.5)
TNI2	2.04 (6.1)	2.16 (5.9)
TNI3u	2.07 (5.9)	2.18 (5.4)
TNI3	2.04 (6.1)	2.16 (5.5)
Paris+TBF	2.06 (6.1)	2.17 (5.6)
AV18+TBF	2.06 (6.1)	2.17 (5.5)
SCL3$\Lambda\Sigma$	2.06 (5.9)	2.17 (5.5)

5.2. *Mass–radius relation*

We now solve the following Tolman–Oppenheimer–Volkov (TOV) equation to obtain the M–R relationship by using EOSs with and without the hadron–quark crossover:

$$\frac{dP}{dr} = -\frac{G}{r^2}\left(M(r) + 4\pi P r^3\right)(\varepsilon + P)\left(1 - 2GM(r)/r\right)^{-1},$$
$$M(r) = \int_0^r 4\pi r'^2 \varepsilon(r')dr', \tag{13}$$

where we have assumed spherical symmetry, with r being the radial distance from the center of the star.

In Fig. 11(a), we show the M–R relationship for various H-EOSs with hyperons whose onset is denoted by the filled circles. The crosses denote the points where maximum masses are realized: In all cases, $M_{\max}$ does not reach $2M_\odot$ due to the softening of EOS by the hyperon mixture.

In Fig. 11(b), we show the M–R relationship with the EOS interpolated between H-EOS and Q-EOS: For the H-EOS, we consider the same EOSs as shown in Fig. 11(a), while, for the Q-EOS, we adopt the HK parameter set with $g_V = G_S$ as a typical example. The crossover window is fixed to be $(\bar{\rho}, \Gamma) = (3\rho_0, \rho_0)$. Cases for different parameters in Q-EOS as well as for different window parameters are discussed in the next subsection.

The red lines in Fig. 11(b) correspond to the cases with TNI2u and TNI2, the blue lines correspond to TNI3u and TNI3, and the green lines correspond to SCL3$\Lambda\Sigma$ and AV18+TBF. The onset of strangeness and the maximum mass are denoted by filled circles and the crosses, respectively. Irrespective of the H-EOSs, the interpolated EOS can sustain a hybrid star with $M_{\max} > 2M_\odot$: A smooth crossover around $\rho \sim 3\rho_0$ and a stiff Q-EOS due to repulsive vector interaction are two fundamental reasons for this fact. Also, we note that the radius of the hybrid star with the interpolated EOS is in the range $R = (11 \pm 1)$ km for $0.5 < M/M_\odot < 2.0$, except for the SCL3$\Lambda\Sigma$ case.[1] Such a narrow window of R independent of the values of M is consistent with the phenomenological constraints on R based on recent observations of both transiently accreting and bursting sources [52,53].

In Table 3, we show the maximum mass and the associated central density of a hybrid star with the interpolated EOS with $g_V = G_S$ and $g_V = 1.5G_S$. In all combinations of H-EOS and Q-EOS, $M_{\max}$ exceeds $2M_\odot$ with the central density, $\rho_c = (5.4\text{–}6.1)\rho_0$.

Let us now turn to the internal structure of the hybrid star, in particular its strangeness content. From the location of the filled circles in Fig. 11(b), one finds that the flavor-independent universal

[1] The reason that the SCL3$\Lambda\Sigma$ case is different from others can easily be seen from Fig. 2: The pressure P of SCL3$\Lambda\Sigma$ is nearly twice as large as that of the other EOSs at $\rho = (1-2)\rho_0$. This leads to a larger R for light NSs.

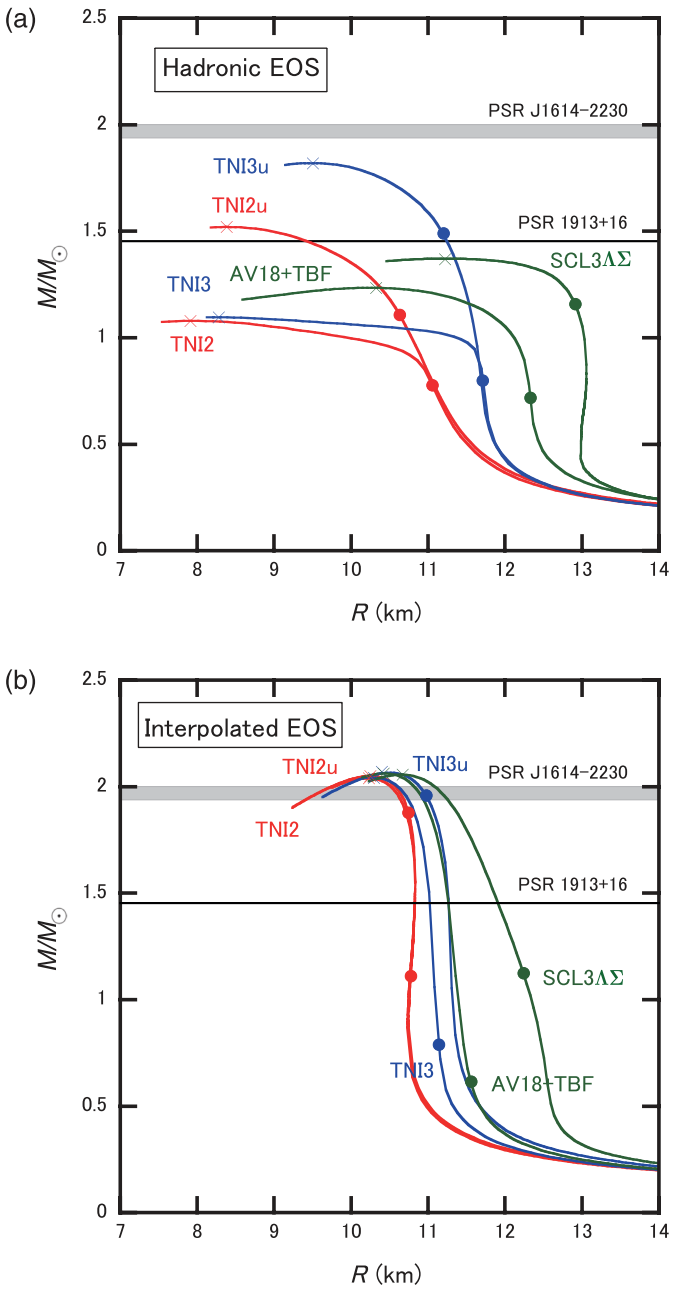

Fig. 11. M–R relationships. (a) M–R relationships with various H-EOSs including hyperons. Solid red lines: TNI2u (universal three-body force with $\kappa = 250$ MeV) and TNI2 (three-nucleon force with $\kappa = 250$ MeV). Solid blue lines: TNI3u (universal three-body force with $\kappa = 300$ MeV) and TNI3 (three-nucleon force with $\kappa = 300$ MeV) [34,35]. Solid green lines: AV18+TBF (G-matrix approach with hyperons) [37] and SCL3$\Lambda\Sigma$ (relativistic mean field model with chiral SU(3) symmetry) [40]. The gray band denotes $M = (1.97 \pm 0.04)M_\odot$ for PSR J1614-2230. The solid black line denotes $M = 1.44M_\odot$ for PSR 1913+16. (b) M–R relationship with the EOS interpolated between H-EOS in (a) and Q-EOS with the HK parameter set and $g_V = G_S$, with the window parameters $(\bar{\rho}, \Gamma) = (3\rho_0, \rho_0)$. The colors of each line are the same as those in (a).

three-baryon repulsion in TNI2u and TNI3u increases the onset density of the strangeness inside the hybrid star. This can be seen more explicitly by plotting the radial profile of the hybrid star: The upper panels of Fig. 12 show the ρ–r relationships for $2M_\odot$ and $1.44M_\odot$ hybrid stars with TNI2 (left) and TNI2u (right). The threshold densities of the strangeness given in Table 1 are indicated by

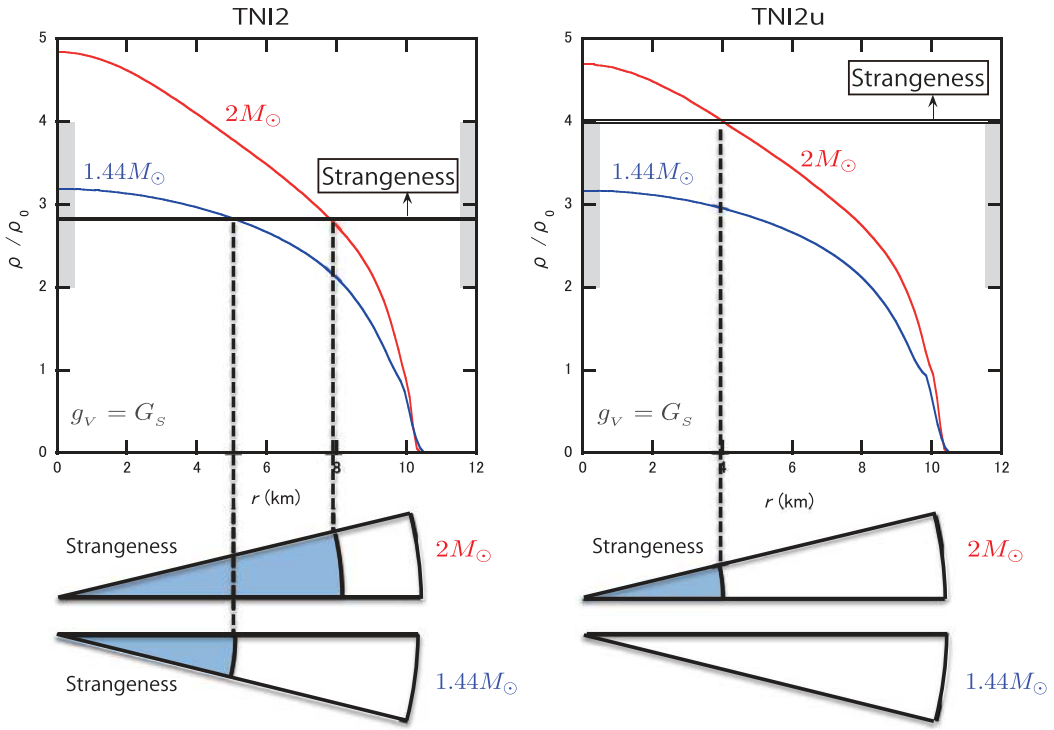

Fig. 12. Density profiles $\rho(r)$, with r being the distance from the center for a $2.0M_\odot$ star (red line) and a $1.44M_\odot$ star (blue line). In the upper left panel, the TNI2 H-EOS and Q-EOS with $g_V = G_S$ and the HK parameter set are used in the interpolation with the window parameters $(\bar{\rho}, \Gamma) = (3\rho_0, \rho_0)$, while, in the upper right panel, the TNI2u H-EOS and the Q-EOS above are used. The double line shows the density above which the strangeness appears. The lower illustrations show the internal structure. Only the shaded regions contain strangeness degrees of freedom.

double lines. In our interpolated EOSs, the above stars turn out to have almost the same radius. The lower illustrations of Fig. 12 show the cross sections of the corresponding hybrid stars.

These figures imply that, even if the mass and the radius are the same, the strangeness content of the hybrid stars can be quite different. This point is of particular interest for the cooling problem of NSs. As is well known, NSs with a Y-mixed core undergo extremely rapid cooling due to the efficient ν-emission processes called "hyperon direct URCA" (Y-Durca, e.g., $\Lambda \to p + e^- + \bar{\nu}_e$, $p + e^- \to \Lambda + \nu_e$) and are cooled very rapidly below the thermal X-ray detection limit. Therefore, for NSs consisting of pure hadronic components with Y, only the very light-mass NSs ($M < (1.0 - 1.2)M_\odot$, as in Fig. 3) can escape from Y-Durca rapid cooling. This indicates the unlikely situation that all the NSs whose T_s are observed should be light-mass stars, in spite of the fact that the observed mass distribution is centered around $(1.4 - 1.5)M_\odot$ [2]. In contrast, in the case of the hybrid star with $g_V = G_S(1.5G_S)$ under consideration, NSs as heavy as up to $1.9(2.0)M_\odot$ can avoid this rapid cooling, allowing the T_s-observed NSs to be from the light-mass to heavy-mass stars ($M \leq (1.9 - 2.0)M_\odot$, as in Fig. 13).[2]

It is in order here to comment on the relationship between the maximum mass and the nuclear incompressibility κ. From the properties of finite nuclei, the nuclear incompressibility κ is estimated

[2] However, in the case of the hybrid star with smooth crossover, "quark direct URCA" (Q-Durca) instead of Y-Durca may take place in the crossover region. The effect of spin-singlet and spin-triplet color superconductivity on this Q-Durca is an interesting open question to be studied.

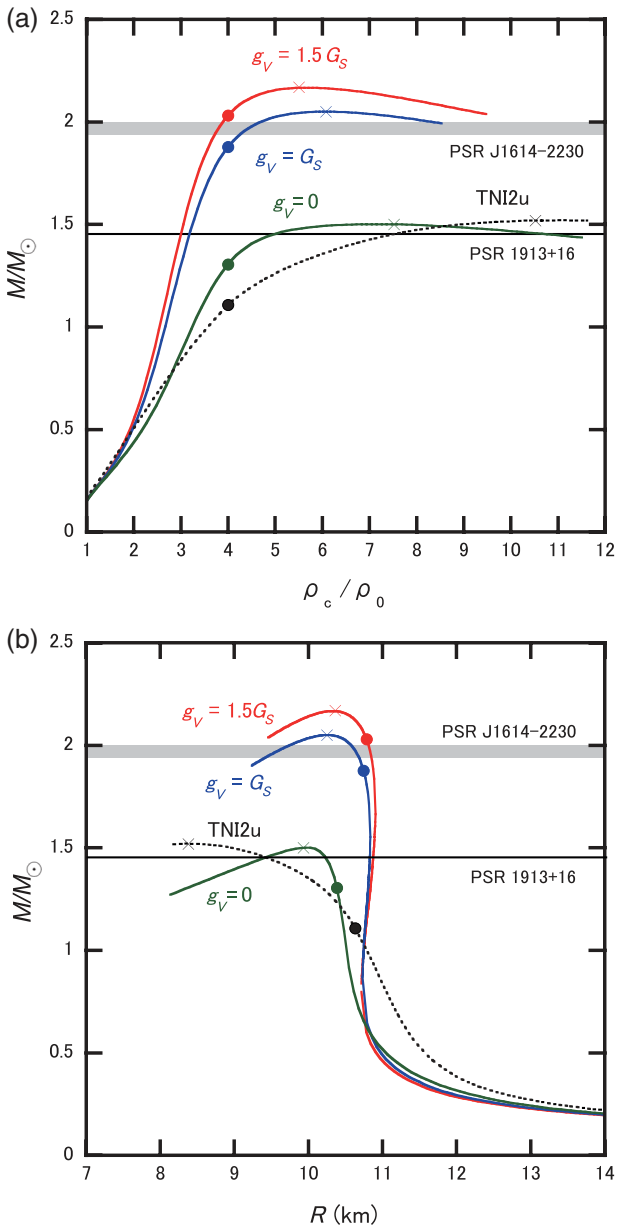

Fig. 13. (a) M–ρ_c relationships with the interpolated EOSs. We adopt the HK parameter set for the Q-EOS with various $g_V/G_S = 0, 1.0, 1.5$. The crossover windows are fixed to be $(\bar{\rho}, \Gamma) = (3\rho_0, \rho_0)$. The cross symbols denote the points of $M_{\max}$, while the filled circles denote the points beyond which the strangeness appears. The gray band denotes $M = (1.97 \pm 0.04)M_\odot$ for PSR J1614-2230. The solid black line denotes $M = 1.44M_\odot$ for PSR 1913+16. (b) M–R relationships with the interpolated EOSs.

to be (240 ± 20) MeV [54]. The interpolated EOSs with TNI2 and TNI2u are consistent with this empirical κ, and yet they can reach $M_{\max} > 2M_\odot$. In other words, what is important to sustain massive hybrid stars is not the value of the incompressibility, but the stiffness of the EOS at and above $\sim 3\rho_0$.

5.3. *Dependence on Q-EOS*

To see how the hybrid star structure changes with the stiffness of Q-EOS, we plot the M–ρ_c relationship for $g_V/G_S = 0, 1.0, 1.5$ with the HK parameter set in Fig. 13(a). We take TNI2u for H-EOS

Table 4. The values of $M_{\max}/M_\odot$ (ρ_c/ρ_0) for $g_V/G_S = 1.0, 1.5, 2.0$ with $(\bar{\rho}, \Gamma) = (3\rho_0, \rho_0)$ and TNI2u. The parameter sets of the NJL model, HK, RKH, and LKW, are given in Table 2.

Q-EOS	$g_V = G_S$	$g_V = 1.5G_S$	$g_V = 2G_S$
HK	2.05 (6.1)	2.17 (5.5)	2.24 (5.4)
RKH	1.99 (6.2)	2.12 (5.8)	2.20 (5.4)
LKW	1.72 (7.5)	1.87 (6.7)	1.97 (6.3)

Table 5. $M_{\max}/M_\odot$ (ρ_c/ρ_0) for the HK parameter set with the flavor-dependent repulsion G_S. The crossover window is $(\bar{\rho}, \Gamma) = (3\rho_0, \rho_0)$ and the hadronic EOS is TNI2u.

$G_V = 1.5G_S$	$G_V = 2.25G_S$	$G_V = 3.0G_S$
1.87 (6.6)	1.99 (6.2)	2.07 (5.8)

Table 6. $M_{\max}/M_\odot$ (ρ_c/ρ_0) under variation of the parameters $\bar{\rho}$ and Γ, which characterize the crossover window. H-EOS and Q-EOS are obtained from TNI2u and the HK parameter set, respectively. Columns without numbers are the excluded cases corresponding to $\bar{\rho} - 2\Gamma < \rho_0$ in Sect. 4.

	$\Gamma/\rho_0 = 1$		$\Gamma/\rho_0 = 2$	
$\bar{\rho}$	$g_V = G_S$	$g_V = 1.5G_S$	$g_V = G_S$	$g_V = 1.5G_S$
$3\rho_0$	2.05 (6.1)	2.17 (5.5)	–	–
$4\rho_0$	1.89 (7.2)	1.97 (6.8)	–	–
$5\rho_0$	1.73 (8.2)	1.79 (8.0)	1.74 (8.0)	1.80 (7.7)
$6\rho_0$	1.60 (9.6)	1.64 (9.3)	1.62 (9.2)	1.66 (9.0)

and the same crossover window as in Fig. 11. For comparison, the M–ρ_c relationship with TNI2u only is plotted by the dashed line. Figure 13(b) shows the corresponding M–R relations. As anticipated, $M_{\max}$ increases as g_V increases. In Table 4, we show how $M_{\max}$ and ρ_c depend on the choice of g_V and the choice of the NJL parameter set. Although the parameter dependence is not entirely negligible, a massive hybrid star is possible for sufficiently large values of g_V.

Finally, we consider the flavor-dependent vector interaction proportional to G_V given in Eq. (1). In the high-density limit where u, d, s quarks have equal population, $\langle u^\dagger u\rangle = \langle d^\dagger d\rangle = \langle s^\dagger s\rangle$, the g_V interaction and the G_V interaction make the same contribution to the pressure in the mean-field approximation if we make the following identification: $G_V = \frac{3}{2} g_V$. Motivated by this relation, we show $M_{\max}$ and ρ_c for $G_V/G_S = 1.5, 2.25, 3.0$ in Table 5. For the density relevant to the cores of hybrid stars, the flavor SU(3) limit is not yet achieved due to the s-quark mass (see Fig. 4). Therefore, the EOS for the flavor-dependent repulsion with $G_V = \frac{3}{2} g_V$ is softer than the flavor-independent repulsion with g_V. This can be seen by comparing the corresponding values in Table 5 and those in Table 4. In any case, a massive hybrid star is possible for sufficiently large values of G_V.

5.4. Dependence on crossover window

In Table 6, we show $M_{\max}$ and ρ_c for different choices of the crossover window parameterized by $\bar{\rho}$ and Γ. TNI2u and the HK parameter set are adopted for H-EOS and Q-EOS, respectively. As the crossover window becomes lower and/or wider in baryon density, the interpolated EOS becomes stiffer and $M_{\max}$ becomes larger. To be compatible with the observed massive NS with $M = (1.97 \pm 0.04) M_\odot$, the crossover needs to occur in $(2 - 4)\rho_0$.

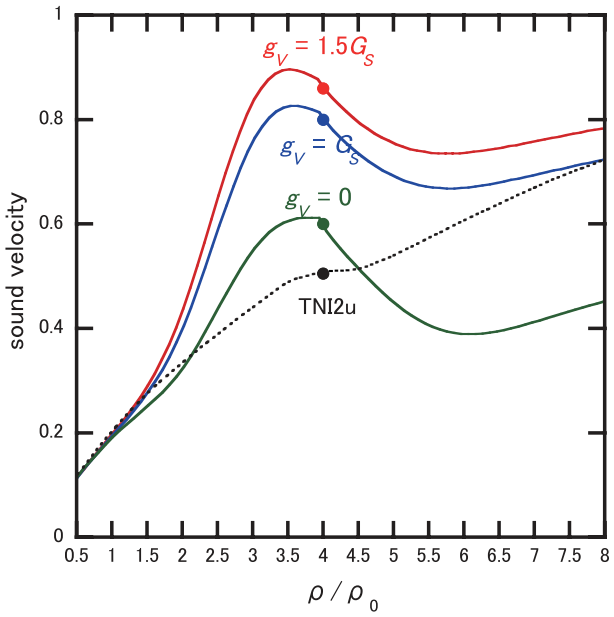

Fig. 14. Sound velocity v_S as a function of baryon density ρ. Solid lines: v_S–ρ obtained from the interpolated EOS between the H-EOS with TNI2u and the Q-EOS with $g_V/G_S = 0, 1.0, 1.5$. The crossover window is $(2-4)\rho_0$. Dotted line: as above for the pure H-EOS with TNI2u. The filled circles denote the points beyond which strangeness starts to appear.

5.5. *Sound velocity of interpolated EOS*

One of the measures to quantify the stiffness of the EOS is the sound velocity $v_S = \sqrt{dP/d\varepsilon}$. In Fig. 14, we plot v_S for our interpolated EOS with $g_V/G_S = 0, 1.0, 1.5$ as a function of ρ. The kinks of v_S at $\rho \simeq 4\rho_0$ are caused by the softening of the EOS by the appearance of strangeness. The enhancement of v_S of the interpolated EOS relative to the pure hadronic EOS takes place just at and above the crossover window.

5.6. *Stability of the hybrid star*

The neutron star is gravitationally stable if the average adiabatic index $\bar{\Gamma}$ satisfies the inequality [55]

$$\bar{\Gamma} = \frac{\int_0^R \Gamma P d^3r}{\int_0^R P d^3r} > \frac{4}{3} + \lambda \frac{GM}{R}. \tag{14}$$

Here $\Gamma = d \ln P / d \ln \varepsilon$ is the adiabatic index. Also, $\lambda GM/R$, with λ being a numerical constant of order unity, is a general relativistic correction whose magnitude is much less than 1. Since Γ of our H-EOS is about 2 at all densities and Γ of our Q-EOS is larger than 4/3 due to the constituent quark mass and the repulsive vector interaction, Eq. (14) is always satisfied and our hybrid star is gravitationally stable.

6. Neutron star properties with ε-interpolation

In this section we consider an alternative interpolation procedure using the energy density ε as a function of ρ given in Eq. (10).

Shown in Fig. 15 is the energy density interpolated between TNI2u for H-EOS and NJL with $g_V = 0.5G_S$ for Q-EOS. The crossover window is chosen to be $(\bar{\rho}, \Gamma) = (3\rho_0, \rho_0)$ and is shown by the shaded area on the horizontal axis. The pressure obtained from the interpolated energy density

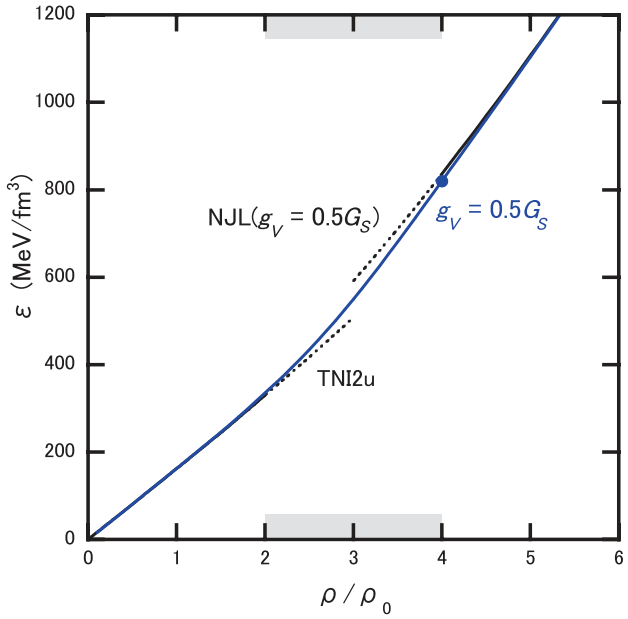

Fig. 15. The interpolated energy density between TNI2u H-EOS and NJL Q-EOS with $g_V = 0.5G_S$ for $(\bar{\rho}, \Gamma) = (3\rho_0, \rho_0)$. Energy density is illustrated by a blue line. The filled circle denotes the threshold density of strangeness.

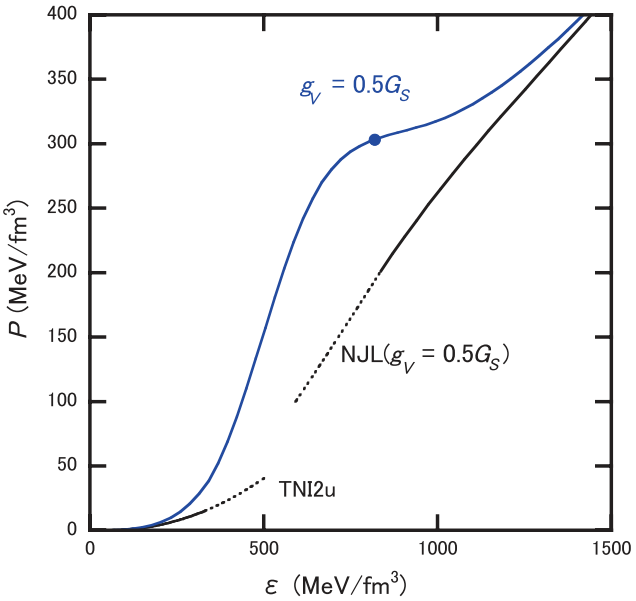

Fig. 16. The pressure obtained from the interpolated energy density in Fig. 15. The pressure is illustrated by a blue line. The filled circle denotes the threshold density of strangeness.

using the thermodynamic relation is shown in Fig. 16. Due to the extra positive term ΔP in Eq. (12), the full pressure is larger than P_H and P_Q in the crossover region with the ε-interpolation procedure. Although ΔP is necessary for thermodynamic consistency, its physical interpretation is not clear at the moment and is left for future studies. In Figs. 17 and 18, we show P as a function of ε and the sound velocity v_S as a function of ρ, respectively. Because of the effect of ΔP, the EOS becomes

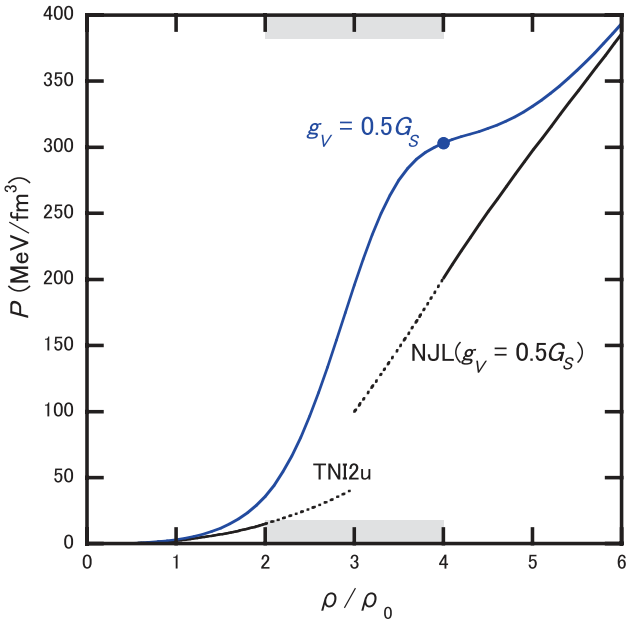

Fig. 17. The relation between the interpolated energy density and the resultant pressure. The parameters are same as in Fig. 16. The filled circle denotes the threshold density of strangeness.

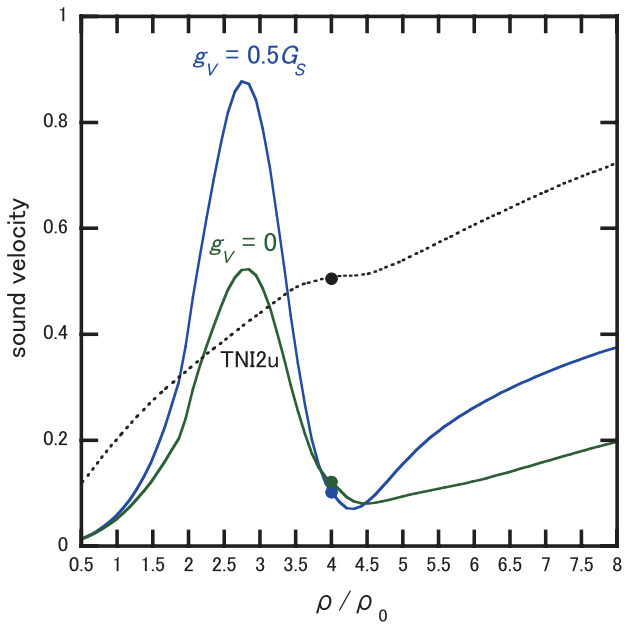

Fig. 18. Sound velocity v_S as a function of baryon density ρ. Solid lines: v_S–ρ obtained from the interpolated EOS between the H-EOS with TNI2u and the Q-EOS with $g_V/G_S = 0, 0.5$. The crossover window is $(2-4)\rho_0$. Dotted line: as above for the pure H-EOS with TNI2u. The filled circles denote the points beyond which strangeness starts to appear.

stiff and v_S is enhanced, particularly in the crossover region. Thus, the maximum mass of the neutron star would become large even for a moderate value of g_V.

In Fig. 19(a), we plot the M–ρ_c relationship between TNI2u for H-EOS and NJL Q-EOS for $g_V/G_S = 0, 0.5$ with the HK parameter set. We choose the crossover window as $(\bar{\rho}, \Gamma) = (3\rho_0, \rho_0)$.

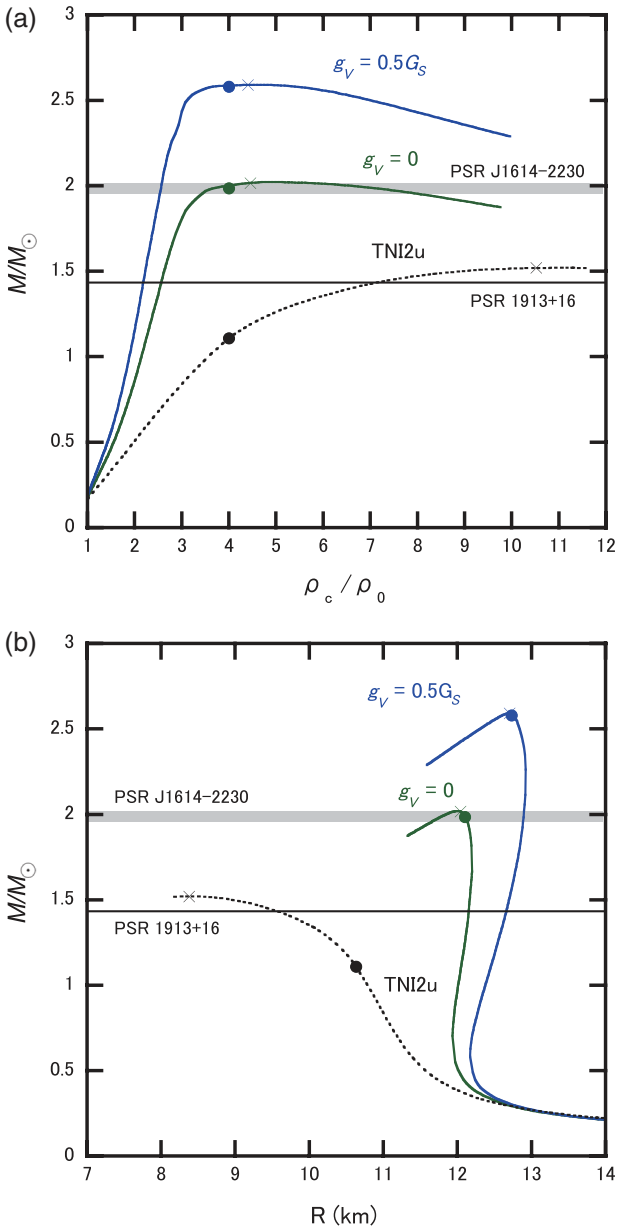

Fig. 19. (a) M–ρ_c relationships with the interpolated EOSs. We adopt the HK parameter set for the Q-EOS with various $g_V/G_S = 0, 0.5$. The crossover windows are fixed to be $(\bar{\rho}, \Gamma) = (3\rho_0, \rho_0)$. The cross symbols denote the points of $M_{\max}$, while the filled circles denote the points beyond which the strangeness appears. The gray band denotes $M = (1.97 \pm 0.04)M_\odot$ for PSR J1614-2230. The solid black line denotes $M = 1.44M_\odot$ for PSR 1913+16. (b) M–R relationships with the interpolated EOSs.

For comparison, the M–ρ_c relationship with TNI2u only is shown by the dashed line. Figure 13(b) shows the corresponding M–R relationships. As anticipated from Fig. 18, the maximum mass is larger than the P-interpolation case for a given g_V.

In Table 7, we show $M_{\max}$ and ρ_c for different H-EOSs, vector-type interactions g_V, and choices of crossover window parameterized by $\bar{\rho}$ and Γ. The ε-interpolation makes the EOS stiffen more drastically than the P-interpolation. Even for $(g_V, \bar{\rho}) = (0, 3\rho_0)$ and $(g_V, \bar{\rho}) = (0.5, 5\rho_0)$, the maximum mass $M_{\max}$ can exceed $1.97M_\odot$.

Table 7. $M_{\max}/M_\odot$ (ρ_c/ρ_0) for different choices of H-EOS, stiffness of Q-EOS, and crossover window.

	$g_V = 0$		$g_V = 0.5G_S$	
H-EOS	$(\bar{\rho}, \Gamma) = (3\rho_0, \rho_0)$	$(5\rho_0, 2\rho_0)$	$(3\rho_0, \rho_0)$	$(5\rho_0, 2\rho_0)$
TNI2u	2.02 (4.5)	1.86 (8.7)	2.59 (4.4)	2.25 (6.1)
TNI2	2.02 (5.8)	1.84 (9.1)	2.59 (4.3)	2.23 (6.8)
TNI3u	1.99 (4.8)	1.89 (8.5)	2.57 (4.7)	2.26 (6.0)
TNI3	1.97 (5.8)	1.80 (6.3)	2.55 (4.5)	2.21 (7.3)
Paris+TBF	1.92 (4.8)	1.75 (6.5)	2.52 (4.7)	2.17 (6.5)
AV18+TBF	1.94 (4.7)	1.75 (7.2)	2.53 (4.7)	2.19 (6.1)
SCL3$\Lambda\Sigma$	1.85 (4.8)	1.73 (7.7)	2.46 (4.7)	2.15 (6.8)

7. Summary and concluding remarks

Recent observation of a two-solar mass NS presents a challenging problem of how to reconcile the stiff EOS suggested from the observational side with the soft EOS due to hyperon-mixing from the theoretical side. In this paper we have studied this problem on the basis of the percolation picture from hadronic matter with hyperons to quark matter with strange quarks. We have constructed an EOS by interpolation between the H-EOS at lower densities and the Q-EOS at higher densities, and found that hybrid stars could have $M_{\max} \sim 2M_\odot$, compatible with observation. This conclusion is in contrast to the conventional EOS for hybrid stars derived through the Gibbs construction, in which the resultant EOS always becomes softer than the hadronic EOS and thereby leads to a smaller $M_{\max}$.

Our qualitative conclusion is insensitive to the choice of different types of H-EOS and different types of vector interaction in Q-EOS as long as (i) the crossover between the hadronic matter and the quark matter proceeds in a relatively low-density region, ($\rho = (2-4)\rho_0$), and (ii) the quark matter is strongly interacting and stiff ($g_V/G_S \sim 1$). These conditions applied to the P-interpolation procedure can be relaxed further if ε-interpolation is adopted. We found that the the sound velocity v_S, which increases rapidly in the crossover window for $g_V/G_S \geq 1$, can nicely characterize the stiffening of the interpolated EOS and associated enhancement of $M_{\max}$.

The idea of rapid stiffening of the EOS starting from $2\rho_0$ opens a possibility that the experimental nuclear incompressibility $\kappa = (240 \pm 20)$ MeV at $\rho \sim \rho_0$ is compatible with the existence of massive neutron stars. Also, the idea may well be checked by independent laboratory experiments with medium-energy heavy-ion collisions.

Although the M–R relationship and $M_{\max}$ are insensitive to the existence of universal three-body repulsion, the onset density of strangeness is rather sensitive to such repulsion. If we have three-body repulsion acting universally among baryons, most of the hybrid stars with $M \leq (1.9-2.0)M_\odot$ are free from the extremely efficient hyperon direct-Urca cooling process and can avoid contradicting observations.

Finally, we remark that the crossover region may contain richer non-perturbative phases such as color superconductivity, inhomogeneous structures, and so on [1]. How these structures, as well as the associated cooling processes, affect the results of the present paper would be an interesting future problem to be examined.

Acknowledgements

We thank Wolfram Weise, Gordon Baym, David Blaschke, and Mark Alford for discussions. T.T. thanks Ryozo Tamagaki, Toshitaka Tatsumi, and Shigeru Nishizaki for discussions and interest in this work. We also thank K. Tsubakihara and A. Ohnishi for providing us with the numerical data for the SCL3 EOS. This research was

supported in part by a MEXT Grant-in-Aid for Scientific Research on Innovative Areas (No.2004:20105003), by a JSPS Grant-in-Aid for Scientific Research (B) No.22340052, and by RIKEN 2012 Strategic Programs for R & D.

Appendix. EOS tables

In this Appendix, we show the concrete values of pressure P and energy density ε as a function of baryon density $x \equiv \rho/\rho_0$ for H-EOSs, Q-EOSs, and interpolated EOSs.

In Table A1, we show H-EOSs with hyperons: TNI2, TNI2u, TNI3, TNI3u [34,35], AV18+TBF [37], and SCL3$\Lambda\Sigma$ [40].

In Table A2, NJL Q-EOSs with the HK parameter set for various vector interactions $g_V/G_S =$ 0, 1.0, 1.5 are listed in each row [44].

Table A1. Pressure P (MeV/fm^3) and energy density ε (MeV/fm^3) as a function of baryon density $x \equiv \rho/\rho_0$ for various hadronic EOSs with hyperons [34,35,37,40].

	TNI2		TNI3		TNI2u		TNI3u	
x	P	ε	P	ε	P	ε	P	ε
1.0	2	162	3	162	2	162	3	162
1.5	7	245	9	246	7	245	9	246
2.0	15	330	20	332	15	330	20	332
2.5	26	418	32	422	26	418	38	422
3.0	40	508	40	513	42	508	61	516
3.5	48	600	48	606	62	601	92	615
4.0	57	693	58	700	87	697	131	718
4.5	67	787	69	795	112	797	174	827
5.0	80	882	82	892	140	899	224	941
5.5	93	979	96	990	173	1005	283	1060
6.0	109	1078	113	1090	211	1113	353	1185
6.5	127	1177	131	1191	255	1226	433	1316
7.0	147	1278	152	1293	304	1341	525	1454
7.5	169	1381	175	1397	360	1461	629	1599
8.0	193	1485	200	1503	422	1584	746	1751
8.5	219	1590	227	1610	492	1712	876	1911
9.0	248	1698	256	1719	568	1843	1020	2079
9.5	278	1807	287	1829	651	1979	1178	2256
10.0	311	1917	321	1942	743	2120	1352	2441

	Paris+TBF		AV18+TBF		SCL3$\Lambda\Sigma$		
x	P	ε	P	ε	x	P	ε
0.471	0.370	71.2	0.432	71.2	1.02	5.85	167
0.941	2.41	148	2.59	148	1.51	14.6	251
1.18	4.63	187	4.94	187	2.04	28.9	346
1.76	15.5	287	15.5	288	2.51	41.5	434
2.35	31.2	404	29.0	399	3.02	53.5	531
2.94	45.7	503	44.2	505	3.54	67.8	635
3.53	62.3	617	59.9	623	4.07	84.0	740
4.12	79.0	735	75.3	729	4.57	101	841
4.71	99.9	853	94.4	858	5.01	118	933
5.29	117	965	112	970	5.62	144	1063
5.88	145	1128	139	1122	6.02	162	1150
6.47	168	1240	159	1223	6.60	191	1278
7.06	188	1369	181	1341	7.07	216	1384
7.65	213	1470	205	1459	7.58	244	1499
8.24	242	1599	239	1616	8.12	276	1625
8.82	279	1745	270	1745	8.50	300	1715
9.41	307	1874	302	1879	9.11	339	1860
10.0	347	2031	328	1986	9.54	368	1965

In Table A3, EOSs obtained by the interpolation of pressure between the TNI2u H-EOS and the NJL Q EOS with the HK parameter set with $g_V/G_S = 0, 1.0, 1.5$ for $(\bar{\rho}, \Gamma) = (3\rho_0, \rho_0)$ are listed.

In Table A4, EOSs obtained by the interpolation of energy density between the TNI2u H-EOS and the NJL Q EOS with the HK parameter set with $g_V/G_S = 0, 1.0, 1.5$ for $(\bar{\rho}, \Gamma) = (3\rho_0, \rho_0)$ are listed.

Table A2. Pressure P (MeV/fm^3) and energy density ε (MeV/fm^3) as a function of baryon density $x \equiv \rho/\rho_0$ for NJL Q-EOSs with the HK parameter set for $g_V = G_S$ [44].

	$g_V/G_S = 0$		$g_V/G_S = 1$		$g_V/G_S = 1.5$	
x	P	ε	P	ε	P	ε
1.0	−0.7633	179.2	8.390	188.3	12.97	192.9
1.5	−1.397	268.1	19.20	288.7	29.49	299.0
2.0	6.721	357.8	43.33	394.5	61.64	412.8
2.5	28.71	451.3	85.91	508.5	114.5	537.1
3.0	58.56	550.0	140.9	632.4	182.1	673.6
3.5	91.96	654.0	204.1	766.2	260.1	822.2
4.0	127.5	762.8	274.0	909.3	347.2	982.5
4.5	158.2	876.1	343.6	1061	436.2	1154
5.0	182.8	992.3	411.6	1221	526.0	1335
5.5	203.0	1111	479.9	1388	618.3	1526
6.0	221.0	1231	550.5	1561	715.2	1725
6.5	238.9	1353	625.6	1740	819.0	1933
7.0	258.3	1476	706.8	1925	931.0	2149
7.5	279.8	1601	794.7	2115	1052	2373
8.0	303.7	1727	889.5	2313	1182	2605
8.5	330.0	1854	991.3	2516	1322	2846
9.0	358.4	1984	1100	2725	1471	3096
9.5	389.9	2114	1215	2941	1628	3354
10	421.3	2247	1337	3163	1794	3620

Table A3. Pressure P (MeV/fm^3) and energy density ε (MeV/fm^3) as a function of baryon density $x \equiv \rho/\rho_0$ for EOSs obtained by the interpolation of pressure between the TNI2u H-EOS and the NJL Q EOS with the HK parameter set with $g_V/G_S = 0, 1.0, 1.5$ for the $(\bar{\rho}, \Gamma) = (3\rho_0, \rho_0)$ case. For practical reasons, in the hadronic phase, we fit pressure as a function $a\rho^b$ by using the least-squares method.

	TNI2						TNI2u					
	$g_V/G_s = 0$		$g_V/G_s = 1$		$g_V/G_s = 1.5$		$g_V/G_s = 0$		$g_V/G_s = 1$		$g_V/G_s = 1.5$	
x	P	ε	P	ε	P	ε	P	ε	P	ε	P	ε
1.0	2.480	168.9	2.645	179.5	2.727	184.8	2.480	168.8	2.645	179.4	2.727	184.8
1.5	6.737	255.4	7.714	271.5	8.202	279.6	6.737	255.3	7.714	271.4	8.202	279.5
2.0	13.90	343.7	18.26	366.0	20.45	377.1	13.90	343.6	18.26	365.9	20.45	377.0
2.5	26.93	434.4	42.31	464.4	50.00	479.4	26.93	434.3	42.31	464.3	50.00	479.3
3.0	49.03	528.1	90.22	569.3	110.8	589.8	50.19	528.5	91.38	569.7	112.0	590.3
3.5	80.26	629.2	162.2	687.2	203.2	716.2	83.90	627.5	165.8	685.5	206.8	714.5
4.0	119.2	733.0	248.2	814.2	312.7	854.8	122.7	731.6	251.7	812.8	316.2	853.4
4.5	153.9	841.7	330.4	952.0	418.7	1007	156.0	841.7	332.6	952.0	420.9	1007
5.0	181.0	953.8	405.7	1099	518.0	1171	182.1	954.0	406.8	1099	519.1	1171
5.5	202.3	1068	477.3	1252	614.8	1344	202.8	1069	477.8	1253	615.4	1345
6.0	220.7	1185	549.4	1413	713.7	1527	220.9	1185	549.6	1413	714.0	1527
6.5	238.8	1303	625.1	1579	818.3	1718	238.9	1303	625.3	1580	818.4	1718
7.0	258.2	1422	706.6	1752	930.7	1917	258.3	1422	706.6	1752	930.8	1918
7.5	279.8	1543	794.6	1931	1052	2125	279.8	1543	794.6	1931	1052	2125
8.0	303.7	1665	889.5	2115	1182	2341	303.7	1665	889.5	2116	1182	2341
8.5	330.0	1789	991.3	2306	1322	2565	330.0	1789	991.3	2307	1322	2566
9.0	358.4	1914	1100	2503	1471	2798	358.4	1915	1100	2504	1471	2799
9.5	389.0	2041	1215	2707	1628	3039	388.9	2042	1215	2707	1628	3040
10.0	421.3	2170	1337	2916	1794	3289	421.3	2170	1337	2917	1794	3290

Table A4. Pressure P (MeV/fm^3) and energy density ε (MeV/fm^3) as a function of baryon density $x \equiv \rho/\rho_0$ for EOSs obtained by the interpolation of energy density between the TNI2u H-EOS and the NJL Q EOS with the HK parameter set with $g_V/G_S = 0, 0.5$ for the $(\bar{\rho}, \Gamma) = (3\rho_0, \rho_0)$ case.

	TNI2				TNI2u			
	$g_V/G_s = 0$		$g_V/G_s = 0.5$		$g_V/G_s = 0$		$g_V/G_s = 0.5$	
x	P	ε	P	ε	P	ε	P	ε
1.0	2.844	162.3	3.088	162.4	2.844	162.3	3.088	162.4
1.5	9.940	245.1	11.82	245.6	9.941	245.1	11.83	245.6
2.0	25.71	333.3	35.59	335.5	25.72	333.3	35.59	335.5
2.5	60.74	426.2	96.55	433.9	60.74	426.2	96.55	433.9
3.0	113.6	528.5	196.0	549.1	113.2	529.0	195.6	549.6
3.5	155.8	639.2	274.0	680.2	156.9	639.8	275.0	680.8
4.0	178.6	754.4	304.6	818.9	177.2	755.1	303.2	819.6
4.5	190.5	871.8	316.5	960.1	188.2	872.3	314.1	960.6
5.0	200.5	990.4	333.0	1103	198.4	990.7	330.9	1103
5.5	211.9	1109	359.6	1248	210.5	1110	358.1	1248
6.0	225.3	1231	394.5	1395	224.4	1231	393.6	1395
6.5	240.9	1353	436.4	1546	240.4	1353	435.9	1546
7.0	259.2	1476	484.4	1700	258.9	1476	484.1	1700
7.5	280.2	1601	538.1	1858	280.1	1601	538.0	1858
8.0	303.9	1727	597.0	2020	303.8	1727	596.9	2020
8.5	330.1	1854	660.8	2185	330.0	1854	660.8	2185
9.0	358.5	1984	729.2	2354	358.5	1984	729.2	2354
9.5	389.0	2115	802.0	2528	389.0	2115	802.0	2528
10.0	421.3	2247	879.0	2705	421.3	2247	878.9	2705

References

[1] K. Fukushima and T. Hatsuda, Rep. Prog. Phys. **74**, 014001 (2011).
[2] J. M. Lattimer and M. Prakash, Phys. Rep. **442**, 109 (2007).
[3] T. Takatsuka, Prog. Theor. Phys. Suppl. **156**, 84 (2004) and references therein.
[4] S. Weissenborn, D. Chatterjee, and J. Schaffner-Bielich, Nucl. Phys. A **881**, 62 (2010).
[5] H. J. Schulze, A. Polls, A. Ramos, and I. Vidana, Phys. Rev. C **73**, 058801 (2006).
[6] T. Takatsuka, S. Nishizaki, and R. Tamagaki, AIP Conf. Proc. **1011**, 209 (2008).
[7] F. Özel, D. Psaltis, S. Ransom, P. B. Demorest, and M. Alford, Astrophys. J. **724**, 1199 (2010).
[8] H. Djapo, B. J. Schaefer, and J. Wambach, Phys. Rev. C **81**, 035803 (2010).
[9] A. Kurkela, P. Romatschke, A. Vuorinen, and B. Wu, arXiv:1006.4062 [astro-ph.HE].
[10] T. Nagae, Prog. Theor. Phys. Suppl. **185**, 299 (2010).
[11] H. Tamura, Prog. Theor. Phys. Suppl. **185**, 315 (2010).
[12] K. Nakazawa and H. Takahashi, Prog. Theor. Phys. Suppl. **185**, 335 (2010).
[13] T. Inoue et al. [HAL QCD Collaboration], Nucl. Phys. A **881**, 28 (2012).
[14] P. B. Demorest, T. Pennucci, S. M. Ranson, M. S. E. Roberts, and J. W. T. Hessels, Nature **467**, 1081 (2010).
[15] K. Kim, H. K. Lee, and M. Rho, Phys. Rev. C **84**, 035810 (2011).
[16] S. Weissenborn, D. Chatterjee, and J. Schaffner-Bielich, Phys. Rev. C **85**, 065802 (2012).
[17] T. Klahn, D Blaschke, and R. Lastowiecki, Acta Phys. Pol. B **5** 757 (2012).
[18] S. Weissenborn, I. Sagert, G. Pagliara, M. Hempel, and J. Schaffner-Bielich, Astrophys. J. **740**, L14 (2011).
[19] L. Bonanno and A. Sedrakian, Astron. Astrophys. **539**, A16 (2012).
[20] H. Chen, M. Baldo, G. F. Burgio, and H. J. Schulze, Phys. Rev. D **86**, 045006 (2012).
[21] S. Schramm, V. Dexheimer, R. Negreiros, T. Schurhoff, and J. Steinheimer, arXiv:1202.5113 [astro-ph.SR].
[22] D. L. Whittenbury, J. D. Carroll, A. W. Thomas, K. Tsushima, and J. R. Stone, arXiv:1204.2614 [nucl-th].
[23] T. Katayama, T. Miyatsu, and K. Saito, Astrophys. J. Suppl. Ser. **203**, 22 (2012).
[24] T. Takatsuka, T. Hatsuda, and K. Masuda, AIP Conf. Proc. **1484**, 406 (2012).
[25] M. A. Baranov, Phys. Rep. **464**, 71 (2008).

[26] G. Baym, Physica A **96**, 131 (1979).
[27] T. Celik, F. Karsch, and H. Satz, Phys. Lett. B **97**, 128 (1980).
[28] T. Schafer and F. Wilczek, Phys. Rev. Lett. **82**, 3956 (1999).
[29] K. Fukushima, Phys. Lett. B **591**, 277 (2004).
[30] G. Baym, T. Hatsuda, M. Tachibana, and N. Yamamoto, J. Phys. G **35**, 104021 (2008).
[31] K. Maeda, G. Baym, and T. Hatsuda, Phys. Rev. Lett. **103**, 085301 (2009).
[32] V. Kalogera and G. Baym, Astrophys. J. **470**, L61 (1996).
[33] K. Masuda, T. Hatsuda, and T. Takatsuka, Astrophys. J. **794**, 12 (2013).
[34] S. Nishizaki, Y. Yamamoto, and T. Takatsuka, Prog. Theor. Phys. **105**, 607 (2001).
[35] S. Nishizaki, Y. Yamamoto, and T. Takatsuka, Prog. Theor. Phys. **108**, 703 (2002).
[36] B. Friedman and V. R. Pandharipande, Nucl. Phys. A **361**, 502 (1981).
[37] M. Baldo, G. F. Burgio, and H. J. Schulze, Phys. Rev. C **61**, 055801 (2000).
[38] Z. H. Li and H. J. Schulze, Phys. Rev. C **78**, 028801 (2008).
[39] H. J. Schulze and T. Rijken, Phys. Rev. C **84**, 035801 (2011).
[40] K. Tsubakihara, H. Maekawa, H. Matsumiya, and A. Ohnishi, Phys. Rev. C **81**, 065206 (2010).
[41] A. Akmal, V. R. Pandharipande, and D. G. Ravenhall, Phys. Rev. C **58**, 1804 (1998).
[42] U. Vogel and W. Weise, Prog. Part. Nucl. Phys. **27**, 195 (1991).
[43] S. P. Klevansky, Rev. Mod. Phys. **64**, 649 (1992).
[44] T. Hatsuda and T. Kunihiro, Phys. Rep. **247**, 221 (1994).
[45] M. Buballa, Phys. Rep. **407**, 205 (2005).
[46] M. Asakawa and K. Yazaki, Nucl. Phys. A **504**, 668 (1989).
[47] N. M. Bratovic, T. Hatsuda, and W. Weise, Phys. Lett. B **719**, 131 (2013).
[48] O. Lourenco, M. Dutra, T. Frederico, A. Delfino, and M. Malheiro, Phys. Rev. D **85**, 097504 (2012).
[49] M. Asakawa and T. Hatsuda, Phys. Rev. D **55**, 4488 (1997).
[50] J. P. Blaizot and J. Y. Ollitrault, Phys. Lett. B **191**, 21 (1987).
[51] J. P. Blaizot and J. Y. Ollitrault, Phys. Rev. D **36**, 916 (1987).
[52] A. W. Steiner, J. M. Lattimer, and E. F. Brown, Astrophys. J. **765**, L5 (2013).
[53] F. Özel, A. Gould, and T. Guver, Astrophys. J. **748**, (2012).
[54] S. Shlomo, V. M. Kolomietz, and G. Colò, Eur. Phys. J. A **30**, 23 (2006).
[55] S. L. Shapiro and S. A. Teukolsky, *Black Holes, White Dwarfs, and Neutron Stars: The Physics of Compact Objects* (Wiley, New York, 1983).